

Pure nematic state in an iron-based superconductor

Y. Kubota,^{1,*} F. Nabeshima,² K. Nakayama,^{3,4} H. Ohsumi,¹ Yoshikazu Tanaka,¹ K. Tamasaku,^{1,5} T. Suzuki,⁶ K. Okazaki,⁶ T. Sato,^{3,7} A. Maeda,² and M. Yabashi^{1,5}

¹RIKEN Spring-8 Center, 1-1-1 Kouto, Sayo, Hyogo 679-5148, Japan

²Department of Basic Science, University of Tokyo, 3-8-1 Komaba, Meguro, Tokyo 153-8902, Japan

³Department of Physics, Graduate School of Science, Tohoku University, Sendai 980-8578, Japan

⁴Precursory Research for Embryonic Science and Technology,

Japan Science and Technology Agency, Tokyo 102-0076, Japan

⁵Japan Synchrotron Radiation Research Institute (JASRI), 1-1-1 Kouto, Sayo, Hyogo 679-5198, Japan

⁶Institute for Solid State Physics, The University of Tokyo, Kashiwa, Chiba 277-8581, Japan

⁷Advanced Institute for Materials Research (WPI-AIMR), Tohoku University, Sendai 980-8577, Japan

(Dated: August 29, 2022)

Lattice and electronic states of thin FeSe films on LaAlO₃ substrates are investigated in the vicinity of the nematic phase transition. No evidence of structural transition is found in x-ray diffraction below $T^* \sim 90$ K, while results obtained from resistivity measurement and angle-resolved photoemission spectroscopy show a clear appearance of the nematic state. These results indicate realization of a pure nematic state in the iron-based superconductor and provide conclusive evidence that the nematic state originates from the electronic degrees of freedom. This pure nematicity in the thin film also implies difference in the electron-lattice interaction from bulk FeSe crystals. Thus, FeSe films provide valuable playgrounds where the pure response of “bare” electron systems free from the electron-lattice interaction is observed, and should make important contribution to investigate nematicity and its relation to superconductivity.

Iron-based superconductors have been extensively studied since the discovery of superconductivity in LaFeAsO_{1-y}F_y [1, 2]. The iron-chalcogenide superconductors, such as FeSe, have also been attracting a great interest owing to the simplest crystal structure and the absence of antiferromagnetism compared with other iron-based superconductors [3–7]. Furthermore, FeSe has exotic features concerning the critical temperature (T_c). Although T_c is only ~ 8 K at ambient pressure [3], T_c increases to $40 \sim 50$ K by physical pressure [8–12], chemical manipulations [13–18], and electric field [19–21]. Monolayer FeSe films exhibit T_c above 65 K [22, 23]. To understand the origin of the Cooper pair formation in iron-based superconductors, it is important to reveal the relation between superconductivity and exotic properties owing to the electronic degrees of freedom.

The electronic nematicity, where the electronic system spontaneously breaks a rotation symmetry accompanied by a structural variation and a development of antiferromagnetism, is one of the intriguing states shown in almost all families of iron-based superconductors [24–31]. Figure 1 shows variations of the lattice and the band structures of FeSe at the nematic transition. The lattice exhibits a tetragonal-to-orthorhombic structural transition at $T^* \sim 90$ K [3, 32–34]. On the other hand, the shape of the Fermi surface and the band diagram change across T^* due to the lifting of d_{xz} and d_{yz} orbital degeneracy [35–42]. Around the M point, the d_{xz} band shifts downward along the $(0, 0)$ - $(0, \pi)$ direction of the untwinned crystal, while the d_{yz} band shifts upward along the $(0, 0)$ - $(\pi, 0)$ direction, leading to the breaking of the four-fold rotational symmetry. For the twinned FeSe sample, these two bands can be observed simultaneously, as shown in

Figs. 1(e) and 1(f). Because the nematic phase is adjacent to the superconducting phase in the phase diagram, nematicity is considered to be closely related to superconductivity [4–7, 31]. Thus, the investigation of the origin and physical properties of nematicity will lead to clarification of the unsettled superconducting mechanisms. Which degrees of freedom are the origin of nematicity is one of the important issues.

In this Letter, we have investigated the lattice and electronic properties of thin FeSe films on LaAlO₃ (LAO) substrates in the vicinity of the nematic phase transition with x-ray diffraction (XRD), resistivity measurement, and angle-resolved photoemission spectroscopy (ARPES). FeSe is an ideal platform to study the origin of nematicity because it undergoes a structural transition without any magnetic order [43]. The electronic degrees of freedom have been considered to be more dominant in the nematic transition than the lattice degree of freedom because the energy splitting of the electronic system in the nematic state is larger than that estimated from the lattice variation [31]. However, it has been difficult to discuss the origin of nematicity in a view of complete decoupling between the electronic and lattice degrees of freedom. From our observation of a pure electronic nematic state not accompanied by the structural phase transition, we show conclusive evidence that the nematic state originates from the electronic degrees of freedom.

FeSe thin films in this study were grown on LAO (001) substrates using a pulsed laser deposition method with a KrF laser ($\lambda = 248$ nm) [44, 45]. The growth temperature and growth rate were 500°C and ~ 1 nm/min, respectively. The thickness of the film for XRD measurement was approximately 50 nm. Much thicker films

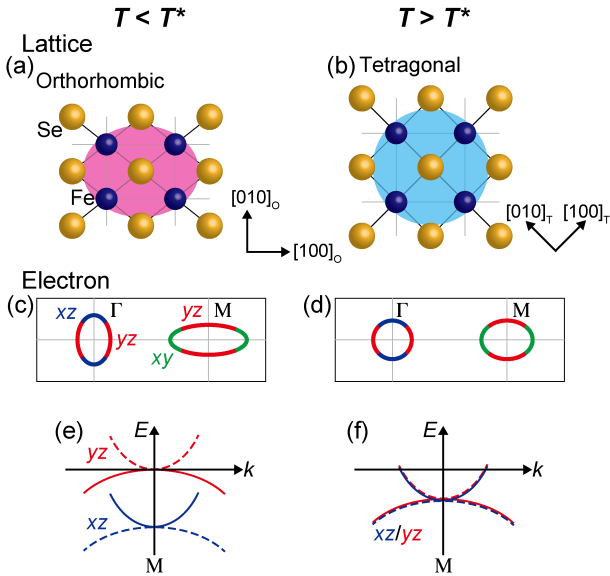


FIG. 1. Comparisons of (a), (b) the lattice structure, (c), (d) the Fermi surface around the Γ and M points, and (e), (f) the band diagram around the M point of FeSe between the nematic state ($T < T^*$) and the normal state ($T > T^*$). The pink and blue circles in (a) and (b) indicate the appearance of electronic nematicity. The blue, red, and green curves in (c)-(f) indicate the d_{xz} , d_{yz} , and d_{xy} orbital bands, respectively. Solid and dashed curves in (e) and (f) represent the band dispersion along the $(0,0)-(\pi,0)$ and $(0,0)-(0,\pi)$ directions (long and short Fe-Fe directions) of the untwinned crystal, respectively [36].

(thickness > 300 nm) were prepared for ARPES measurements so that the films were easily cleaved. Figure 2(a) shows the XRD θ - 2θ scan of an FeSe film on LAO at room temperature, demonstrating the c -axis orientation of the film. The c -axis lattice constant was 5.50 Å, which is slightly shorter than those of bulk samples ($5.521 \sim 5.525$ Å [46, 47]). The shorter c -axis length indicates an in-plane tensile strain in the film [48]. Figure 2(b) shows the rocking curve of the 001 reflection of the film. The two peak structure is due to the twin of the rhombohedral LAO substrate.

ARPES measurements were performed with Scienta-Omicron-DA30 and MBS-A1 electron analyzers at BL28A in Photon Factory [49] and BL7U in UVSOR, respectively. To excite photoelectrons, we used circularly polarized 56-eV photons and linearly polarized 21-eV photons. The energy and angular resolutions were set to be $12 \sim 30$ meV and 0.3 degrees, respectively. A clean surface for ARPES measurements was obtained by cleaving FeSe films in situ in an ultrahigh vacuum better than 1×10^{-10} Torr. The thickness of the films after the cleavage was ~ 70 nm estimated by transmission electron microscopy measurements. The Fermi level (E_F) of the films was referenced to that of a gold film electrically

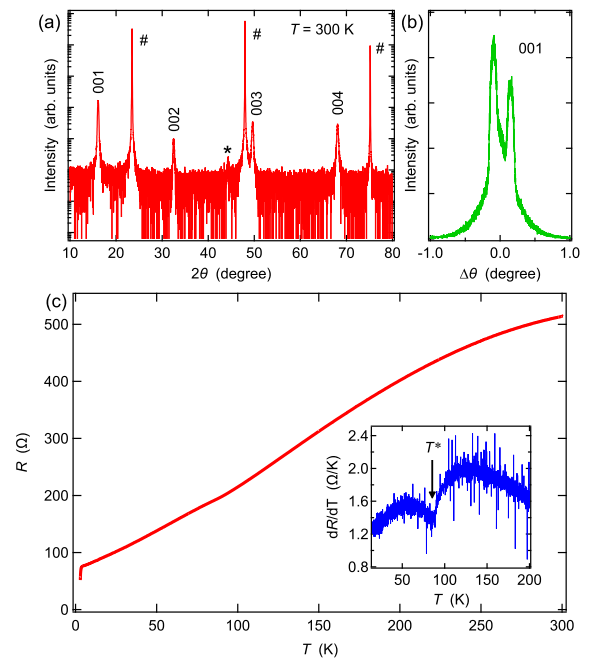


FIG. 2. Results of characterization of the FeSe film on LAO. (a) XRD pattern obtained at room temperature. The number and asterisk signs represent peaks from the LAO substrate and the sample holder made of stainless, respectively. (b) A rocking curve of the 001 reflection of the FeSe film. (c) Temperature dependence of the resistance, R , of the FeSe film. The inset shows the temperature dependence of dR/dT of the FeSe film. The arrow shows the nematic transition temperature, T^* .

contacted on the sample holder.

An XRD measurement under low temperatures was performed at BL19LXU of SPring-8 [50]. The photon energy of the x-ray beam was 10 keV monochromatized by a pair of cryogenically cooled Si (111) crystals. The energy resolution was $\sim 1 \times 10^{-4}$. The x-ray intensity of the 336 Bragg reflection in the tetragonal structure was detected with a NaI scintillation counter and an x-ray CMOS image sensor, SOPHIAS [51]. This high index reflection was chosen to detect the change in lattice structure with high precision. The distance between the sample and SOPHIAS was ~ 2 m resulting in the angle resolution being 8.6×10^{-4} degrees. The sample temperature was cooled with a cryostat to a minimum of 6 K.

Figure 2(c) shows the temperature dependence of the resistance, R , of an FeSe on LAO, which was grown at the same time as the sample for the XRD measurement under low temperatures. Because of the tensile strain, the superconducting transition temperature (T_c^{onset} of 3.2 K) is lower than that of bulk samples [48, 52]. A resistive anomaly, which is clearly indicated by a dip structure in the temperature derivative of the resistance [inset of Fig. 2(c)], suggests the nematic transition at

$T^* \sim 90$ K [35].

To corroborate the emergence of nematicity in the FeSe films on LAO, we have investigated the evolution of the electronic structure across T^* by using ARPES. Figure 3(a) shows a representative ARPES intensity plot at low temperatures below T^* ($T = 30$ K) measured along the Γ - M cut of the Brillouin zone. The near- E_F band structure around the Γ point consists of two hole-like bands; the inner one has the top of dispersion slightly below E_F , whereas the outer one crosses E_F . According to previous studies of FeSe bulk crystals and thin films, these bands are attributed to the Fe $3d_{xz}/d_{yz}$ orbitals [35–37, 42], and their energy separation at the Γ point (20 \sim 30 meV) signifies the lifting of orbital degeneracy due to spin-orbit coupling (SOC) [53]. Around the M point, there are two holelike bands with the top at binding energies (E_B s) of ~ 10 and ~ 60 meV. While these bands also have the d_{xz}/d_{yz} orbital character, the magnitude of their energy separation ($\Delta E \sim 50$ meV) is much larger than the SOC gap at the Γ point. Such a large ΔE between the d_{xz}/d_{yz} orbitals at the M point is a hallmark of the nematic state [Fig. 1(e)] [35–42] and hence supports the formation of nematicity at low temperatures in the FeSe films on LAO. As seen from the ARPES intensity plot at $T = 130$ K in Fig. 3(b), ΔE at the M point, i.e., nematicity, is suppressed at high temperatures. To examine this point in detail, we plot in Figs. 3(c) and 3(d) the temperature dependence of the ARPES spectrum at the M point and its second-derivative intensity, respectively. Upon increasing temperature, the band at higher E_B shifts toward E_F , whereas the band at lower E_B shifts away from E_F , leading to a decrease of ΔE (note that finite ΔE at high temperatures likely reflects the SOC gap opening [53] and/or a contribution of the d_{xy} orbital [41, 54, 55]). The temperature dependence of ΔE displayed in Fig. 3(e) indicates that nematicity in the FeSe films on LAO is gradually suppressed in the temperature range between 80 K and 100 K, in reasonable agreement with the onset of nematicity around $T^* \sim 90$ K estimated from the electrical resistivity measurements [Fig. 2(c)].

Figure 4 shows the results of the XRD measurement at the 336 Bragg reflection in the tetragonal structure. Hereafter, we describe this reflection as 336_T , while the reflections in the orthorhombic structure use the subscript of O. We measured the temperature dependence of diffraction from 6 K to 120 K. In bulk samples, the 336_T peak has been known to split into a doublet of 606_O and 066_O due to the structural transition below T^* [3, 32–34]. The split angle at $T = 6$ K is evaluated as ~ 1.3 degrees in 2θ using the lattice constants of the bulk sample reported in the previous study [32]. However, we could not observe the splitting in a θ - 2θ scan detected with the scintillation counter, as shown in Fig 4(a). For more precise discussion, we also measured the 336_T peak with SOPHIAS placed further away from

the sample than the scintillation counter. Figure 4(b) shows a temperature dependence of the XRD profile at the 336_T with SOPHIAS. Although the detector has a high angle resolution of 8.6×10^{-4} degrees, no splitting was also observed. Rather than splitting, the peak width decreases with decreasing temperature. Furthermore, if the peak splits, the intensity of one of the split peaks should be smaller than the original one. However, as shown in Fig. 4(b), the peak intensity becomes larger at lower temperatures. Therefore, there is no possibility that the splitting angle is too large to observe with the detection area. The multiple peaks that appear regardless of temperature are due to the twin of the rhombohedral LAO substrate, as shown in Fig. 2(b). Note that we also performed θ scans at each temperature and confirmed that there is no splitting. From the above, we can conclude that no structural phase transition occurs in the FeSe thin film on LAO. It is natural to consider that the structural change is suppressed by the strain from the substrate [56].

From the fact that our results from resistivity measurement and ARPES are similar to those of bulk FeSe crystals; there is no doubt that the nematic transition occurs at T^* in the FeSe thin film on LAO. On the other hand, the XRD measurement at low temperatures indicates that no structural phase transition has occurred. Thus, a pure electronic nematicity is realized in the FeSe thin film. This is an evidence that the nematic phase originates only from the electronic degrees of freedom. The effective electron-lattice interaction, λ_{eff} , is given by $\lambda_{\text{eff}} \sim \lambda^2/\omega_{\text{ph}}$, where λ and ω_{ph} are the bare electron-lattice interaction and the phonon frequency, respectively. Therefore, assuming that the lattice deformation is suppressed by the substrate in the thin film and that ω_{ph} is higher than that of bulk crystals, λ_{eff} becomes smaller, which provides a qualitative understanding of the pure nematic transition. The pure nematic state in FeSe films provide valuable playgrounds where the pure response of “bare electron systems free from the electron-lattice interaction is observed. The previous time-resolved experiment, performed by Shimojima *et al.* [57], succeeded in investigating the nature of the nematic state decoupled from the lattice state using a difference in their time scales after optical excitation. In contrast, this study shows that the FeSe films realize it even at the equilibrium state. A rapid increase of T_c when the nematic transition is suppressed by changing the chemical composition in film samples may be related to such bare nature of electrons [58, 59]. The realization of higher T_c at ambient pressure in film samples than bulk crystals may also suggest that phonons do not play a key role for realizing 10–40 K class superconductivity in Fe chalcogenides.

In summary, we discovered the pure electronic nematicity not accompanied by the lattice structural transition in the FeSe thin film on LAO. The result is an

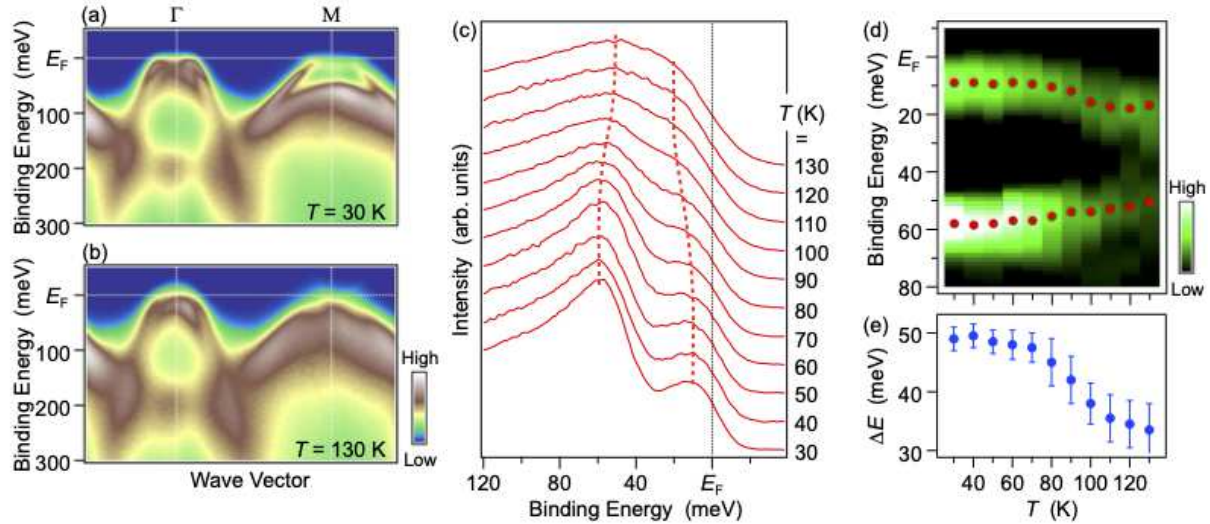


FIG. 3. (a), (b) ARPES intensity as a function of binding energy and wave vector along the Γ - M cut measured at $T = 30\text{ K}$ and 130 K , respectively, with 56-eV photons. (c), (d) Temperature dependence of the ARPES spectrum at the M point and the corresponding second-derivative intensity plot, respectively. Red dashed curves in (c) are a guide for the eyes to trace the energy position of d_{xz}/d_{yz} -derived bands, extracted from the peak position in (d) (red circles). (e) The magnitude of the energy difference between the d_{xz} - and d_{yz} -derived bands at the M point plotted as a function of temperature.

evidence that the origin of nematicity is the electronic degrees of freedom. Compared to bulk crystals, FeSe thin film has advantages in its preparation, such as easy control of composition in elemental substitutions and ease of growing single crystals with large areas [58–60]. With our discovery of the pure nematic state, FeSe thin film is an important platform to investigate the nematic state and the nematic fluctuation, and their relation to superconductivity. Our results open up a novel avenue for studies of iron-based superconductors to unveil the mechanism of superconductivity, increase T_c , and even realize interfacial superconductivity [61, 62].

We thank Dr. Miho Kitamura, Dr. Koji Horiba, Dr. Hiroshi Kumigashira, Dr. Shin-ichiro Ieda, and Dr. Kiyohisa Tanaka for their assistance in the ARPES measurements. We also thank Ataru Ichinose at Central Research Institute of Electric Power Industry for the cross-sectional TEM experiment. The XRD measurement was performed at BL19LXU of SPring-8 with the approval of RIKEN (Proposal No. 20180094, 20190042, and 20200056). This work was supported by JST-PRESTO (No. JPMJPR18L7), JST-CREST (No. JPMJCR18T1), Grant-in-Aid for Scientific Research (JSPS KAKENHI Grant Number: JP20H01847), KEK-PF (Proposal number: 2021S2-001), and UVSOR (Proposal number: 21-679).

- [1] Y. Kamihara, T. Watanabe, M. Hirano, and H. Hosono, *J. Am. Chem. Soc.* **130**, 3296 (2008).
- [2] G. R. Stewart, *Rev. Mod. Phys.* **83**, 1589 (2011).
- [3] F. C. Hsu, J. Y. Luo, K. W. Yeh, T. K. Chen, T. W. Huang, P. M. Wu, Y. C. Lee, Y. L. Huang, Y. Y. Chu, D. C. Yan, and M. K. Wu, *Proc. Natl. Acad. Sci. U.S.A.* **105**, 14262 (2008).
- [4] A. E. Böhmer and A. Kreisel, *J. Phys. Condens. Matter* **30**, 023001 (2018).
- [5] A. I. Coldea and M. D. Watson, *Annu. Rev. Condens. Matter Phys.* **9**, 125 (2018).
- [6] A. Kreisel, P. J. Hirschfeld, and B. M. Andersen, *Symmetry* **12**, 1402 (2020).
- [7] T. Shibauchi, T. Hanaguri, and Y. Matsuda, *J. Phys. Soc. Jpn.* **89**, 102002 (2020).
- [8] Y. Mizuguchi, F. Tomioka, S. Tsuda, T. Yamaguchi, and Y. Takano, *Appl. Phys. Lett.* **93**, 152505 (2008).
- [9] S. Medvedev, T. M. McQueen, I. A. Troyan, T. Palasyuk, M. I. Eremets, R. J. Cava, S. Naghavi, F. Casper, V. Ksenofontov, G. Wortmann, and C. Felser, *Nat. Mater.* **8**, 630 (2009).
- [10] K. Miyoshi, K. Morishita, E. Mutou, M. Kondo, O. Seida, K. Fujiwara, J. Takeuchi, and S. Nishigori, *J. Phys. Soc. Jpn.* **83**, 13702 (2013).
- [11] K. Kothapalli, A. E. Böhmer, W. T. Jayasekara, B. G. Ueland, P. Das, A. Sapkota, V. Taufour, Y. Xiao, E. Alp, S. L. Budko, P. C. Canfield, A. Kreyssig, and A.I. Goldman, *Nat. Commun.* **7**, 12728 (2016).
- [12] J. P. Sun, K. Matsuura, G. Z. Ye, Y. Mizukami, M. Shimozawa, K. Matsubayashi, M. Yamashita, T. Watashige, S. Kasahara, Y. Matsuda, J.-Q. Yan, B. C. Sales, Y. Uwamoto, J.-G. Cheng, and T. Shibauchi, *Nat. Commun.* **7**, 12146 (2016).
- [13] J. Guo, S. Jin, G. Wang, S. Wang, K. Zhu, T. Zhou, M. He, and X. Chen, *Phys. Rev. B* **82**, 180520(R) (2010).

* kubota@spring8.or.jp

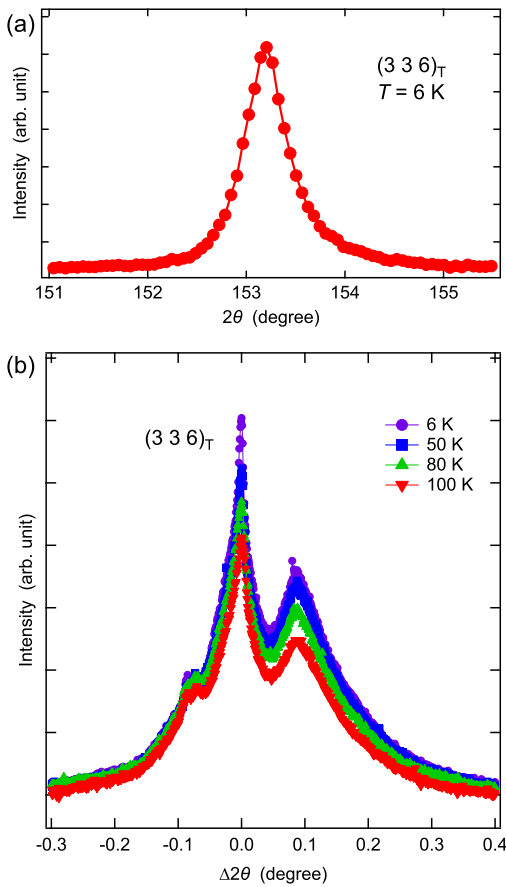


FIG. 4. (a) Result of θ - 2θ scan at the 336_T Bragg reflection obtained at 6 K. (b) Temperature dependence of the x-ray diffraction profile at the 336_T Bragg reflection obtained with SOPHIAS. θ angle was fixed where the diffraction signal shows the maximum value at each temperature. The horizontal axis shows the value relative to the main peak angle.

- [14] Y. Miyata, K. Nakayama, K. Sugawara, T. Sato, and T. Takahashi, *Nat. Mater.* **14**, 775 (2015).
- [15] C. H. P. Wen, H. C. Xu, C. Chen, Z. C. Huang, X. Lou, Y. J. Pu, Q. Song, B. P. Xie, M. Abdel-Hafiez, D. A. Charreev, A. N. Vasiliev, R. Peng, and D. L. Feng, *Nat. Commun.* **7**, 10840 (2016).
- [16] T. P. Ying, X. L. Chen, G. Wang, S. F. Jin, T. T. Zhou, X. F. Lai, H. Zhang, and W. Y. Wang, *Sci. Rep.* **2**, 426 (2012).
- [17] M. Burrard-Lucas, D. G. Free, S. J. Sedlmaier, J. D. Wright, S. J. Cassidy, Y. Hara, A. J. Corkett, T. Lancaster, P. J. Baker, S. J. Blundell, and S. J. Clarke, *Nat. Mater.* **12**, 15 (2013).
- [18] S. Hosono, T. Noji, T. Hatakeyama, T. Kawamata, M. Kato, and Y. Koike, *J. Phys. Soc. Jpn.* **83**, 113704 (2014).
- [19] J. Shiogai, Y. Ito, T. Mitsuhashi, T. Nojima, and A. Tsukazaki, *Nat. Phys.* **12**, 42 (2016).
- [20] K. Hanzawa, H. Sato, H. Hiramatsu, T. Kamiya, and H. Hosono, *Proc. Natl. Acad. Sci. U.S.A.* **113**, 3986 (2016).
- [21] B. Lei, J. H. Cui, Z. J. Xiang, C. Shang, N. Z. Wang, G. J. Ye, X. G. Luo, T. Wu, Z. Sun, and X. H. Chen, *Phys.*

- Rev. Lett. **116**, 077002 (2016).
- [22] Q.-Y. Wang, Z. Li, W.-H. Zhang, Z.-C. Zhang, J.-S. Zhang, W. Li, H. Ding, Y.-B. Ou, P. Deng, K. Chang, J. Wen, C.-L. Song, K. He, J.-F. Jia, S.-H. Ji, Y.-Y. Wang, L.-L. Wang, X. Chen, X.-C. Ma, and Q.-K. Xue, *Chinese Phys. Lett.* **29**, 037402 (2012).
- [23] S. He, J. He, W. Zhang, L. Zhao, D. Liu, X. Liu, D. Mou, Y.-B. Ou, Q.-Y. Wang, Z. Li, L. Wang, Y. Peng, Y. Liu, C. Chen, L. Yu, G. Liu, X. Dong, J. Zhang, C. Chen, Z. Xu, X. Chen, X. Ma, Q. Xue, and X. J. Zhou, *Nat. Mater.* **12**, 605 (2013).
- [24] T.-M. Chuang, M. P. Allan, J. Lee, Y. Xie, N. Ni, S. L. Budko, G. S. Boebinger, P. C. Canfield, and J. C. Davis, *Science* **327**, 181 (2010).
- [25] J.-H. Chu, J. G. Analytis, K. De Greve, P. L. McMahon, Z. Islam, Y. Yamamoto, and I. R. Fisher, *Science* **329**, 824 (2010).
- [26] M. A. Tanatar, E. C. Blomberg, A. Kreyssig, M. G. Kim, N. Ni, A. Thaler, S. L. Budko, P. C. Canfield, A. I. Goldman, I. I. Mazin, and R. Prozorov, *Phys. Rev. B* **81**, 184508 (2010).
- [27] A. Dusza, A. Lucarelli, F. Pfunder, J.-H. Chu, I. R. Fisher, and L. Degiorgi, *Europhys. Lett.* **93**, 37002 (2011).
- [28] M. Yi, D. Lu, J.-H. Chu, J. G. Analytis, A. P. Sorini, A. F. Kemper, B. Moritz, S.-K. Mo, R. G. Moore, M. Hashimoto, W.-S. Lee, Z. Hussain, T. P. Devereaux, I. R. Fisher, and Z.-X. Shen, *Proc. Natl. Acad. Sci. U.S.A.* **108**, 6878 (2011).
- [29] S. Kasahara, H. J. Shi, K. Hashimoto, S. Tonegawa, Y. Mizukami, T. Shibauchi, K. Sugimoto, T. Fukuda, T. Terashima, A. H. Nevidomskyy, and Y. Matsuda, *Nature* **486**, 382 (2012).
- [30] J.-H. Chu, H.-H. Kuo, J. G. Analytis, and I. R. Fisher, *Science* **337**, 710 (2012).
- [31] R. M. Fernandes, A. V. Chubukov, and J. Schmalian, *Nat. Phys.* **10**, 97 (2014).
- [32] S. Margadonna, Y. Takabayashi, M. T. McDonald, K. Kasperkiewicz, Y. Mizuguchi, Y. Takano, A. N. Fitch, E. Suard, and K. Prassides, *Chem. Commun.* 5607 (2008).
- [33] T. M. McQueen, A. J. Williams, P. W. Stephens, J. Tao, Y. Zhu, V. Ksenofontov, F. Casper, C. Felsner, and R. J. Cava, *Phys. Rev. Lett.* **103**, 057002 (2009).
- [34] A. E. Böhmer, F. Hardy, F. Eilers, D. Ernst, P. Adelmann, P. Schweiss, T. Wolf, and C. Meingast, *Phys. Rev. B* **87**, 180505(R) (2013).
- [35] T. Shimojima, Y. Suzuki, T. Sonobe, A. Nakamura, M. Sakano, J. Omachi, K. Yoshioka, M. Kuwata-Gonokami, K. Ono, H. Kumigashira, A. E. Böhmer, F. Hardy, T. Wolf, C. Meingast, H. v. Löhneysen, H. Ikeda, and K. Ishizaka, *Phys. Rev. B* **90**, 121111(R) (2014).
- [36] K. Nakayama, Y. Miyata, G. N. Phan, T. Sato, Y. Tanabe, T. Urata, K. Tanigaki, and T. Takahashi, *Phys. Rev. Lett.* **113**, 237001 (2014).
- [37] S. Y. Tan, Y. Fang, D. H. Xie, W. Feng, C. H. P. Wen, Q. Song, Q. Y. Chen, W. Zhang, Y. Zhang, L. Z. Luo, B. P. Xie, X. C. Lai, and D. L. Feng, *Phys. Rev. B* **93**, 104513 (2016).
- [38] P. Zhang, T. Qian, P. Richard, X. P. Wang, H. Miao, B. Q. Lv, B. B. Fu, T. Wolf, C. Meingast, X. X. Wu, Z. Q. Wang, J. P. Hu, and H. Ding, *Phys. Rev. B* **91**, 214503 (2015).
- [39] M. D. Watson, T. K. Kim, A. A. Haghvirad, N. R. Davies, A. McCollam, A. Narayanan, S. F. Blake, Y. L. Chen, S. Ghannadzadeh, A. J. Schofield, M. Hoesch, C.

Meingast, T. Wolf, and A. I. Coldea, Phys. Rev. B **91**, 155106 (2015).

[40] Y. Suzuki, T. Shimojima, T. Sonobe, A. Nakamura, M. Sakano, H. Tsuji, J. Omachi, K. Yoshioka, M. Kuwata-Gonokami, T. Watashige, R. Kobayashi, S. Kasahara, T. Shibauchi, Y. Matsuda, Y. Yamakawa, H. Kontani, and K. Ishizaka, Phys. Rev. B **92**, 205117 (2015).

[41] M. Yi, H. Pfau, Y. Zhang, Y. He, H. Wu, T. Chen, Z. R. Ye, M. Hashimoto, R. Yu, Q. Si, D.-H. Lee, P. Dai, Z.-X. Shen, D. H. Lu, and R. J. Birgeneau, Phys. Rev. X **9**, 041049 (2019).

[42] G. N. Phan, K. Nakayama, K. Sugawara, T. Sato, T. Urata, Y. Tanabe, K. Tanigaki, F. Nabeshima, Y. Imai, A. Maeda, and T. Takahashi, Phys. Rev. B **95**, 224507 (2017).

[43] P. Dai, Rev. Mod. Phys. **87**, 855 (2015).

[44] Y. Imai, R. Tanaka, T. Akiike, M. Hanawa, I. Tsukada, and A. Maeda, Jpn. J. Appl. Phys. **49**, 023101 (2010).

[45] Y. Imai, T. Akiike, M. Hanawa, I. Tsukada, A. Ichinose, A. Maeda, T. Hikage, T. Kawaguchi, and H. Ikuta, Appl. Phys. Express **3**, 043102 (2010).

[46] T. M. McQueen, Q. Huang, V. Ksenofontov, C. Felser, Q. Xu, H. Zandbergen, Y. S. Hor, J. Allred, A. J. Williams, D. Qu, J. Checkelsky, N. P. Ong, and R. J. Cava, Phys. Rev. B **79**, 014522 (2009).

[47] S. Kasahara, T. Watashige, T. Hanaguri, Y. Kohsaka, T. Yamashita, Y. Shimoyama, Y. Mizukami, R. Endo, H. Ikeda, K. Aoyama, T. Terashima, S. Uji, T. Wolf, H. von Löhneysen, T. Shibauchi, and Y. Matsuda, Proc. Natl. Acad. Sci. U.S.A. **111**, 16309 (2014).

[48] F. Nabeshima, M. Kawai, T. Ishikawa, N. Shikama, and A. Maeda, Jpn. J. Appl. Phys. **57**, 120314 (2018).

[49] M. Kitamura, S. Souma, A. Honma, D. Wakabayashi, H. Tanaka, A. Toyoshima, K. Amemiya, T. Kawakami, K. Sugawara, K. Nakayama, K. Yoshimatsu, H. Kumigashira, T. Sato, and K. Horiba, Rev. Sci. Instrum. **93**, 033906 (2022).

[50] M. Yabashi, T. Mochizuki, H. Yamazaki, S. Goto, H. Ohashi, K. Takeshita, T. Ohata, T. Matsushita, K. Tamasaku, Y. Tanaka, and T. Ishikawa, Nucl. Instruments Methods Phys. Res. Sect. A Accel. Spectrometers, Detect. Assoc. Equip. **467468**, 678 (2001).

[51] T. Hatsui, M. Omodani, T. Kudo, K. Kobayashi, T. Imamura, T. Ohmoto, A. Iwata, S. Ono, Y. Kirihara, T. Kameshima, H. Kasai, N. Miura, N. Kuriyama, M. Okihara, Y. Nagatomo, M. Nagasaki, T. Watanabe, and Makina Yabashi, Proc. of Int. Image Sensor Workshop, 2013 Art. 3.05.

[52] M. Nakajima, Y. Ohata, and S. Tajima, Phys. Rev. Mater. **5**, 044801 (2021).

[53] S. V. Borisenko, D. V. Evtushinsky, Z.-H. Liu, I. Morozov, R. Kappenberger, S. Wurmehl, B. Büchner, A. N. Yaresko, T. K. Kim, M. Hoesch, T. Wolf, and N. D. Zhigadlo, Nature Phys. **12**, 311 (2016).

[54] M. D. Watson, T. K. Kim, L. C. Rhodes, M. Eschrig, M. Hoesch, A. A. Haghaghirad, and A. I. Coldea, Phys. Rev. B **94**, 201107(R) (2016).

[55] L. C. Rhodes, J. Böker, M. A. Müller, M. Eschrig, and I. M. Eremin, npj Quantum Mater. **6**, 45 (2021).

[56] M. J. Wang, J. Y. Luo, T. W. Huang, H. H. Chang, T. K. Chen, F. C. Hsu, C. T. Wu, P. M. Wu, A. M. Chang, and M. K. Wu, Phys. Rev. Lett. **103**, 117002 (2009).

[57] T. Shimojima, Y. Suzuki, A. Nakamura, N. Mitsuishi, S. Kasahara, T. Shibauchi, Y. Matsuda, Y. Ishida, S. Shin, and K. Ishizaka, Nat. Commun. **10**, 1946 (2019).

[58] Y. Imai, Y. Sawada, F. Nabeshima, and A. Maeda, Proc. Natl. Acad. Sci. U.S.A. **112**, 1937 (2015).

[59] Y. Imai, Y. Sawada, F. Nabeshima, D. Asami, M. Kawai, and A. Maeda, Sci. Rep. **7**, 46653 (2017).

[60] F. Nabeshima, T. Ishikawa, K. Oyanagi, M. Kawai, and A. Maeda, J. Phys. Soc. Japan **87**, 73704 (2018).

[61] V. L. Ginzburg, Phys. Lett. **13**, 101 (1964).

[62] D. Allender, J. Bray, and J. Bardeen, Phys. Rev. B **7**, 1020 (1973).